

# 1 **Diurnal Variation of Electron Density in the Saturn** 2 **Ionosphere: Model Comparisons with Saturn Electrostatic** 3 **Discharge (SED) Observations**

4  
5 Luke Moore<sup>1</sup>, Georg Fischer<sup>2,3</sup>, Ingo Müller-Wodarg<sup>1,4</sup>, Marina Galand<sup>1,4</sup>, and Michael  
6 Mendillo<sup>1</sup>

7 <sup>1</sup> Center for Space Physics, Boston University, Boston, MA, USA

8 <sup>2</sup> Space Research Institute, Austrian Academy of Sciences, Graz, Austria

9 <sup>3</sup> Department of Physics and Astronomy, University of Iowa, Iowa City, IA, USA

10 <sup>4</sup> Space and Atmospheric Physics Group, Department of Physics, Imperial College London,  
11 London, UK

## 12 **Abstract**

13  
14 Using the Saturn Thermosphere-Ionosphere Model (STIM), we present a study of the  
15 diurnal variation of electron density, with a focus on direct comparisons with peak  
16 electron densities ( $N_{MAX}$ ) inferred from the low-frequency cutoff of radio emission due to  
17 lightning in the lower atmosphere, called Saturn Electrostatic Discharges (SEDs). It is  
18 demonstrated that photochemistry in the Saturn ionosphere cannot reproduce the SED-  
19 inferred diurnal variation in  $N_{MAX}$ , unless additional production and loss sources outside  
20 of the current best estimates are considered. Additional explanations of the SED-inferred  
21 diurnal variation of  $N_{MAX}$  are presented and analyzed, such as the possibility that the low-  
22 frequency cutoff seen in SEDs is due to the presence of sharp low-altitude layers of  
23 plasma, as frequently seen in radio occultation measurements. Finally, we outline the  
24 observational constraints that must be fulfilled by any candidate explanations of the SED-  
25 inferred diurnal variation of  $N_{MAX}$ .

26  
27 Draft: 17 April 2012

28 Submitted: 20 April 2012

29 Revised:

30 Accepted:

## 31 **1. Introduction**

### 32 *1.1. Detection History*

33           During the 12 November 1980 Voyager 1 encounter with Saturn, the Planetary  
34 Radio Astronomy (PRA) instrument detected mysterious, broadband, short-lived,  
35 impulsive radio emission, termed Saturn Electrostatic Discharges (SEDs) (Warwick et  
36 al., 1981). SED emission was present below 100 kHz, meaning that any intervening  
37 ionosphere would have to have an electron density less than  $\sim 100 \text{ cm}^{-3}$ , counter to the  
38  $\sim 10^4 \text{ cm}^{-3}$  value derived by the radio science team (Tyler et al., 1981). This fact,  
39 combined with the  $\sim 10$  hr periodicity of the SEDs, led Warwick et al. to conclude that  
40 they most likely originated in Saturn's rings, a claim seemingly reinforced by the  
41 detection of a new feature in Saturn's B ring by Voyager 2 (Evans et al., 1982). Burns et  
42 al. (1983), however, argued for an atmospheric source for SEDs, owing primarily to their  
43 similarity with other planetary lightning emission. They noted that shadowing by  
44 Saturn's rings would reduce the local equatorial electron density, thereby providing a  
45 possible explanation of the detection of unusually low frequency SEDs. Kaiser et al.  
46 (1983) supported the case for an atmospheric SED source by demonstrating that a ring  
47 source should have led to a longer SED detection window than was observed.

48           The Radio and Plasma Wave Science (RPWS) instrument aboard Cassini began  
49 detecting SEDs prior to its orbital insertion on 1 July 2004, and has since observed nine  
50 distinct storm periods, separated by quiet periods (with no SED activity) of a few days to  
51 21 months (Fischer et al., 2011a). Shortly after Cassini's arrival at Saturn the Imaging  
52 Science Subsystem instrument detected a large storm system at  $35^\circ$  S latitude that  
53 correlated with the SED recurrence pattern (Porco et al., 2005). Dyudina et al. (2007)

54 extended this finding by presenting three further storm systems where SED observations  
55 were correlated with the rising and setting of a visible storm on the Saturn radio horizon.  
56 Finally, lightning flashes were imaged directly in 2009, providing a convincing  
57 demonstration that SEDs were indeed signatures of storms in Saturn's atmosphere  
58 (Dyudina et al., 2010).

59

### 60 *1.2. SED Characteristics and Ionospheric Implications*

61 SEDs have a large frequency bandwidth, but appear as narrow-banded streaks in  
62 both Voyager PRA and Cassini RPWS dynamic spectra, due to the short duration of the  
63 radio burst and the frequency sampling nature of the receivers. SED burst durations are  
64 typically  $< 0.5$  s, with e-folding times ranging from  $\sim 37$ - $49$  ms (Zarka and Pedersen,  
65 1983; Fischer et al., 2007; Fischer et al., 2008), where the full range encompasses all  
66 SED storms. The number of SEDs detected in an individual storm varies dramatically,  
67 from hundreds to tens of thousands (Fischer et al., 2008), with typical burst rates of a few  
68 hundred per hour (Zarka and Pedersen, 1983; Fischer et al., 2006). *SED storms* are  
69 periods of nearly continuous SED activity, modulated by *episodes* of varying SED  
70 activity. The recurrence period of the episodes within a storm represents the time  
71 between peaks of SED activity; for a single longitudinally confined storm system,  
72 therefore, this period is related to the rotation rate of the atmosphere. Recurrence periods  
73 for Voyager 1 and Voyager 2 SEDs episodes were  $\sim 10$  h 10 min and  $\sim 10$  h 00 min,  
74 respectively (Evans et al., 1981; Warwick et al., 1982), and were therefore thought to  
75 originate from equatorial storm systems (Burns et al., 1983), though none were observed  
76 directly. In contrast, aside from one weak storm in June 2005, all recurrence periods for

77 the Cassini era SED storms are near 10 h 40 min (Fischer et al., 2008), implying a mid-  
78 latitude origin, as confirmed by the 35° S latitude clouds and visible lightning flashes  
79 imaged by Cassini.

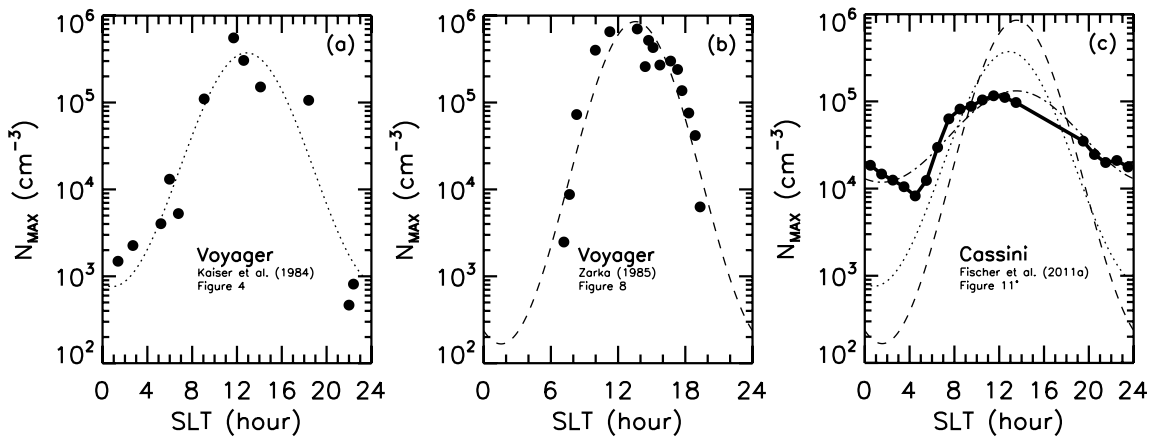
80 SEDs originating from lightning storms deep within Saturn's atmosphere must  
81 ultimately pass through its ionosphere in order to be detected by a spacecraft. Therefore,  
82 the low frequency cutoff of each SED episode provides information about the intervening  
83 plasma densities, as only frequencies larger than the peak electron plasma frequency will  
84 pass through Saturn's ionosphere. Further complications to the SED propagation must  
85 also be considered, however. For example, the spacecraft is very rarely directly overhead  
86 the storm location; an increased angle of incidence ( $\alpha$ ) between the zenith and the  
87 direction of radio wave propagation leads to an increase in the observed cutoff frequency  
88 (e.g., Fischer et al., 2007). In addition, "over horizon" SEDs are observed regularly  
89 (Fischer et al., 2008). These are SEDs that are detected prior to their originating storm  
90 rising above the visible horizon as seen by Cassini, likely a result of ionospheric ducting  
91 (Zarka et al., 2006). This latter point emphasizes that one cannot rely on the assumption  
92 that SEDs traverse a straight line from origin to observer. Nevertheless, with careful  
93 attention to such details, SED measurements can be used to make an estimate of the peak  
94 electron density as a function of local time for Saturn's ionosphere. Such a data product  
95 is highly complementary to the only other remote sensing diagnostic of the mid- and low-  
96 latitude Saturn ionosphere, that of  $N_e(h)$  profiles from radio occultation experiments (e.g.,  
97 Nagy et al., 2006; Kliore et al., 2009). It is important to emphasize that Sun-Saturn-Earth  
98 geometry limits radio occultations to Saturn dawn and dusk, while SEDs can be observed  
99 at all local times.

100 We have focused only on summarizing the basic characteristics of SEDs as they  
 101 relate to the Saturn ionosphere here. For a more complete discussion of the  
 102 complications of SED generation, propagation, and detection the reader is referred to  
 103 Fischer et al. (2011a) and references therein.

104

105 *1.3. Voyager Era Studies*

106 Kaiser et al. (1984) used Voyager SED measurements to derive a diurnal variation  
 107 of the peak electron density in Saturn's ionosphere,  $N_{MAX}$ , of over two orders of  
 108 magnitude. Midnight densities of less than  $10^3 \text{ cm}^{-3}$  were followed by densities in excess  
 109 of  $10^5 \text{ cm}^{-3}$  at noon, with dawn and dusk densities of  $\sim 10^4 \text{ cm}^{-3}$ , in rough agreement with  
 110 the radio occultation data at those local times (e.g., Kliore et al., 1980; Lindal et al.,  
 111 1985). Zarka (1985) derived a slightly larger diurnal variation using a similar analysis.  
 112 Figures 1a and 1b present the Voyager era SED-derived diurnal variation in  $N_{MAX}$  from  
 113 Kaiser et al. (1984), and Zarka (1985), respectively.



114  
 115 **Figure 1.** Diurnal variation in  $N_{MAX}$  derived from Voyager and Cassini SED observations (circles and  
 116 solid curve), along with a least-squares fit to an equation of the form  $\log N_e = A - B \cos(LT - \phi)$  (the  
 117 dotted, dashed and dot-dash curves). (a) Voyager: Figure 4 of Kaiser et al. (1984), (b) Voyager: Figure 8  
 118 of Zarka (1985), (c) Cassini: the diurnal trend from Figure 11 of Fischer et al. (2011a). A straight line has  
 119 been drawn between 13.5 LT and 19.5 LT where there is a relative lack of data (see section 4.1). The dash-  
 120 dotted line represents a fit to the Cassini data set. In addition, the dotted and dashed curves are the fits for  
 121 the Kaiser et al. (1984) and Zarka (1985) diurnal  $N_{MAX}$  trends from the Voyager era, also shown in (a) and  
 122 (b), respectively.

123 Early theoretical models of Saturn's ionosphere predicted  $H^+$  to be the dominant  
124 ion, with a peak density of  $\sim 10^5 \text{ cm}^{-3}$  and a minimal diurnal variation, owing to the long  
125 lifetime of  $H^+$  (e.g., McElroy, 1973). Based on radio occultation measurements of a  $10^4$   
126  $\text{cm}^{-3}$  ionosphere, it had already been recognized that additional losses were required in  
127 the models, such as the conversion of  $H^+$  ions into short-lived molecular ions (Connerney  
128 and Waite, 1984). The first time-dependent model of Saturn's ionosphere to address the  
129 SED-derived diurnal variation of  $N_{\text{MAX}}$  was that of Majeed and McConnell (1996). They  
130 examined a range of possible loss chemistries and forced ion vertical drifts, and could not  
131 find any combination of parameters that would come close to reproducing the SED  
132 observations. Prior to Cassini's arrival at Saturn, Moore et al. (2004) presented a new set  
133 of model results addressing this problem. Their initial results found diurnal variations  
134 similar to those calculated by Majeed and McConnell, and further demonstrated that even  
135 the most drastic or minimal allowable chemical losses, constrained only by Voyager  
136 observations, would not create two order of magnitude variations in  $N_{\text{MAX}}$  in only 5 hours  
137 (i.e., noon  $\leftrightarrow$  midnight).

138

#### 139 *1.4. Outline*

140 Using the Saturn Thermosphere Ionosphere Model (STIM), we present here the  
141 first attempt at reproducing the diurnal variation of  $N_{\text{MAX}}$  obtained from Cassini era  
142 observations. The new constraints provided by Cassini SEDs, and how they differ from  
143 the Voyager ones, are summarized in Section 2. Our model is described in Section 3.  
144 Section 4 presents the model results, and Section 5 discusses possible solutions to the  
145 model-data discrepancy. Finally, concluding thoughts are given in Section 6.

146

## 147 **2. Diurnal Variation of $N_{MAX}$ Derived From Cassini Era SEDs**

148        Even ignoring differences in instrumentation, there are a number of advantages  
149 that Cassini has over the Voyagers when deriving peak electron densities in Saturn's  
150 ionosphere from SEDs. First, the location of the storm cloud tops has been identified for  
151 the majority of Cassini SED storm periods. This means that (a) it is easier to isolate the  
152 local solar time sampled by the SEDs as they propagate through the ionosphere, and (b)  
153 the angle of incidence is known (to an accuracy that depends inversely on the size of the  
154 originating storm). Second, whereas both Voyager spacecraft flew past Saturn in a  
155 matter of days, Cassini has been in orbit since 1 July 2004, and will continue to take data  
156 until 2017 (Spilker, 2012). Such a long term SED data set allows a more complete  
157 coverage in Saturn local time, and also allows study of new topics, such as how the SED-  
158 derived  $N_{MAX}$  diurnal variation responds to changes in solar flux and Saturn season.

159        The vast majority of Cassini era SEDs detected to date originate from storm  
160 systems at  $35^\circ$  S latitude (Fischer et al., 2011a). However, approximately 16 months after  
161 Saturn passed through its equinox (August 2009) towards southern winter, a giant  
162 convective storm developed at  $35^\circ$  N latitude, accompanied by unprecedented levels of  
163 SED activity (Fischer et al., 2011b). Therefore, aside from one small storm which may  
164 have been equatorial, Cassini era SED storms have all been in the hemisphere opposite  
165 the sub-solar point. While the tendency for convective storms to preferentially form near  
166  $\pm 35^\circ$  latitude remains unexplained, it is beneficial for our purposes in that it provides  
167 additional sampling of Saturn's mid-latitude ionosphere.

168 Comprehensive discussion of the Cassini era derivations of peak electron  
169 densities in Saturn's ionosphere to date can be found in Fischer et al. (2011a); we briefly  
170 summarize those findings here. First, while SEDs were detected by both Voyagers for  
171 the few days near closest approach, Cassini's first few years in orbit have revealed that  
172 there are distinctive storm periods separated by periods of SED quiet. Based on 48 SED  
173 episodes between 2004-2009, Figure 1c shows the average diurnal variation of  $N_{MAX}$  at  
174 Saturn for measurements where Cassini was within  $14 R_S$  of Saturn (Fischer et al.,  
175 2011a). In contrast, Voyager 1 observations are based on a few measurement points over  
176 three SED episodes, whereas Voyager 2 data showed a decline in number and intensity of  
177 SEDs with no clear episodic behavior, meaning it could not be used for a similar analysis,  
178 as the storm's position was not well defined (Kaiser et al., 1984). As seen in Figure 9 of  
179 Fischer et al. (2011a), there is good qualitative agreement in the diurnal variations of  
180  $N_{MAX}$  derived from the eight different Cassini storm periods. The maximum  $N_{MAX}$  value  
181 is typically in the early afternoon, while the minimum is in the mid-morning, just before  
182 sunrise, as would be expected (e.g., Moore et al., 2004). Quantitative agreement between  
183  $N_{MAX}$  values for different SED storms is more varied: at a single local time,  $N_{MAX}$  values  
184 derived from different storms can differ by as much as a factor of ten, but are more  
185 typically within a factor of 2-3. On average, the inferred diurnal variation of  $N_{MAX}$  in the  
186 Cassini era is only a factor of ten, from  $\sim 10^4 \text{ cm}^{-3}$  at midnight to  $\sim 10^5 \text{ cm}^{-3}$  at noon. This  
187 is in distinct contrast to the two order of magnitude diurnal variation inferred from  
188 Voyager measurements, where  $N_{MAX}$  values reached below  $10^3 \text{ cm}^{-3}$  during the night. As  
189 no Cassini SEDs have inferred similarly low  $N_{MAX}$  values to date, the Voyager result may  
190 represent an exceptional situation. Finally, Fischer et al. (2011a) also examined trends in



191 derived  $N_{MAX}$  values with solar EUV flux. They found a slight correlation between the  
192 diurnal variation of  $N_{MAX}$  and the EUV flux, and a stronger correlation between the  
193 average peak  $N_{MAX}$  values and the EUV flux, indicating that – as predicted – solar EUV  
194 flux plays a dominant role in ionizing Saturn’s mid-latitude ionosphere.

195

### 196 **3. Modeling Approach**

#### 197 *3.1. The Saturn Thermosphere-Ionosphere Model*

198         The Saturn Thermosphere-Ionosphere Model (STIM) is a suite of 1D, 2D and 3D  
199 models of Saturn’s upper atmosphere. The core of STIM is a 3D global circulation  
200 model (GCM) of the Saturn thermosphere, first described in Müller-Wodarg et al. (2006),  
201 and now updated to include a fully coupled ionosphere (Müller-Wodarg et al., 2012).  
202 Separate 1D (in altitude), and 2D (altitude and latitude) ionospheric modules exist that  
203 use the thermospheric GCM to define background atmospheric parameters not calculated  
204 by the ionospheric modules. These modules include photochemistry, plasma diffusion  
205 (Moore et al., 2004), shadowing due to Saturn’s rings (Mendillo et al., 2005), and a time-  
206 variable water influx (Moore et al., 2006; Moore and Mendillo, 2007). Recently the  
207 ionospheric modules have been coupled with a 1D electron transport code in order to  
208 incorporate the effects of photoelectrons on Saturn’s ionosphere (Galand et al., 2009,  
209 2011), including plasma temperature calculations (Moore et al., 2008), and  
210 parameterizations of the secondary ionization and thermal electron heating rates at Saturn  
211 (Moore et al., 2009). Saturn’s magnetic field is specified with the Saturn Pioneer  
212 Voyager (SPV) model (Davis and Smith, 1990). Calculations using updated magnetic

213 field parameters based on Cassini measurements (e.g., Russell and Dougherty, 2010) do  
214 not show any discernible differences from those using the SPV model.

215 In order to reduce the calculated electron densities to better match radio  
216 occultation observations, models of Saturn’s ionosphere have had to rely on a  
217 combination of charge exchange reactions that remove the long-lived ion  $H^+$  (e.g.,  
218 Majeed and McConnell, 1996; Moses and Bass, 2000). These reactions have typically  
219 been driven by some combination of an assumed influx of water (Connerney and Waite,  
220 1984), and by some assumed fraction of atmospheric molecular hydrogen excited to the  
221 4<sup>th</sup> or higher vibrational level,  $H_2^*$  (McElroy, 1973). As both the influx of  $H_2O$  into  
222 Saturn’s atmosphere and the  $H_2^*$  population are largely unconstrained at present, previous  
223 STIM studies have explored a wide range of possibilities for those parameters (Moore et  
224 al., 2006; 2010), and compared the resulting model calculations with Cassini radio  
225 occultation observations (Nagy et al., 2006; Kliore et al., 2009) in order to find a “best”  
226 match.

227 The effective reaction rate  $k_I^*$  for charge exchange between  $H^+$  and vibrationally  
228 excited  $H_2$  is given by:

$$229 \quad k_1^* = k_1 \frac{[H_2(v \geq 4)]}{[H_2]} \quad [cm^3 s^{-1}] \quad (1)$$

230 where the reaction rate  $k_I$  is taken to be  $1 \times 10^{-9} cm^3 s^{-1}$  (Huestis, 2008), and the initial  
231 population of vibrationally excited hydrogen is taken to be that of Moses and Bass  
232 (2000). As Moses and Bass assumed a  $k_I$  of  $2 \times 10^{-9} cm^3 s^{-1}$ , a factor of two larger than  
233 our rate, the base  $k_I^*$  for our calculations is  $0.5 k_{I MB}^*$ . Any further modifications to  $k_I^*$   
234 throughout this text refer to modifications of this population of vibrationally excited

235 molecular hydrogen,  $[H_2(v \geq 4)]$ , and not the reaction rate  $k_I$  or the background density  
236  $[H_2]$ .

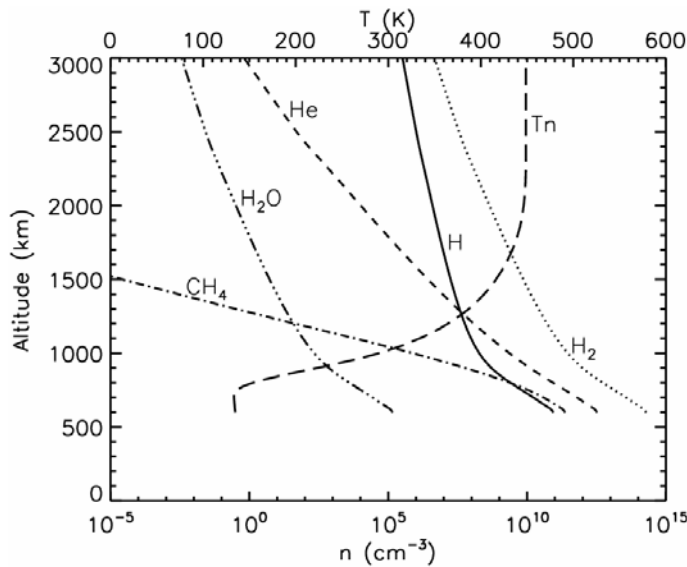
237         Based on model comparisons (Moore et al., 2010) with the latitudinal variation of  
238  $N_{MAX}$  from radio occultations (Kliore et al., 2009), the water influxes used in this study  
239 assume a Gaussian distribution with latitude, peaked at Saturn's equator, with a variance  
240 of  $10^\circ$  latitude. This means that at  $35^\circ$  S latitude, where SED comparison calculations  
241 take place, a peak water influx of  $5 \times 10^6$   $H_2O$  molecules  $cm^{-2} s^{-1}$  (i.e., at the equator)  
242 would be reduced to  $\sim 1.1 \times 10^4$   $cm^{-2} s^{-1}$  – a value too low to significantly affect  
243 ionospheric electron densities. Unless otherwise noted, only the peak water influx at the  
244 equator  $\Phi_{eq}$  is discussed for the remainder of the text, with the above distribution in  
245 latitude assumed.

246         Saturn's lower ionosphere is predicted to be composed of a complex array of  
247 hydrocarbon ions which provide an additional ledge of ionization between Saturn's main  
248 photochemical peak and the homopause (Moses and Bass, 2000). STIM does not include  
249 the hundreds of reactions necessary to fully apportion accurate hydrocarbon ion fractions;  
250 rather it uses a small subset of simplified chemistry that acts predominantly as a sink for  
251 Saturn's major ions,  $H^+$  and  $H_3^+$ . Though the ultimate hydrocarbon ions in STIM's  
252 chemical scheme –  $CH_3^+$ ,  $CH_4^+$ , and  $CH_5^+$ , hereafter designated  $CH_X^+$  – are different  
253 from those that result from a more complete treatment (e.g.,  $C_3H_5^+$  of Moses and Bass,  
254 2000), the calculated electron density is approximately equal (Moore et al., 2004).

255

256 *3.2. Simulations of Diurnal Variation in Electron Density*

257 The background neutral atmosphere, upon which the 1D ionospheric calculations  
 258 are based, comes from the 3D GCM (Müller-Wodarg et al., 2006). While there now  
 259 exists an updated version of the GCM (Müller-Wodarg et al., 2012), we have chosen to  
 260 maintain consistency with previous publications by using the GCM background described  
 261 in Moore et al. (2010). In brief, this simulation is for solar minimum conditions at Saturn  
 262 equinox, and reproduces neutral temperature measurements in the UV (Smith et al., 1983;  
 263 Nagy et al., 2009) and IR (Melin et al., 2007). Altitude profiles of neutral densities and  
 264 temperatures from this background atmosphere are presented in Figure 2.



265 **Figure 2.** Background neutral atmospheric densities and temperature, extracted from the 3D GCM for 35°  
 266 S latitude at local noon. Also shown is the water density profile calculated at 35° S latitude for a  $\Phi_{eq}$  of  
 267  $5 \times 10^6 \text{ cm}^{-2} \text{ s}^{-1}$ .  
 268  
 269

270 The solar declination angle for the 1D ionospheric module calculations is fixed at  
 271  $-8.5^\circ$ , representing the average seasonal condition for the 31 radio occultation  
 272 observations published to date (Nagy et al., 2006; Kliore et al., 2009), and also a fair  
 273 approximation to the average condition for Cassini era SED storms (Fischer et al.,  
 274 2011a). Solar flux at the top of the atmosphere is based on similar average conditions,  
 275 specified using the measurements from the Thermosphere Ionosphere Mesosphere

276 Energetics and Dynamics Solar EUV Experiment (TIMED/SEE) extrapolated to Saturn  
277 (Woods et al., 2000, 2005; Woods, 2008).

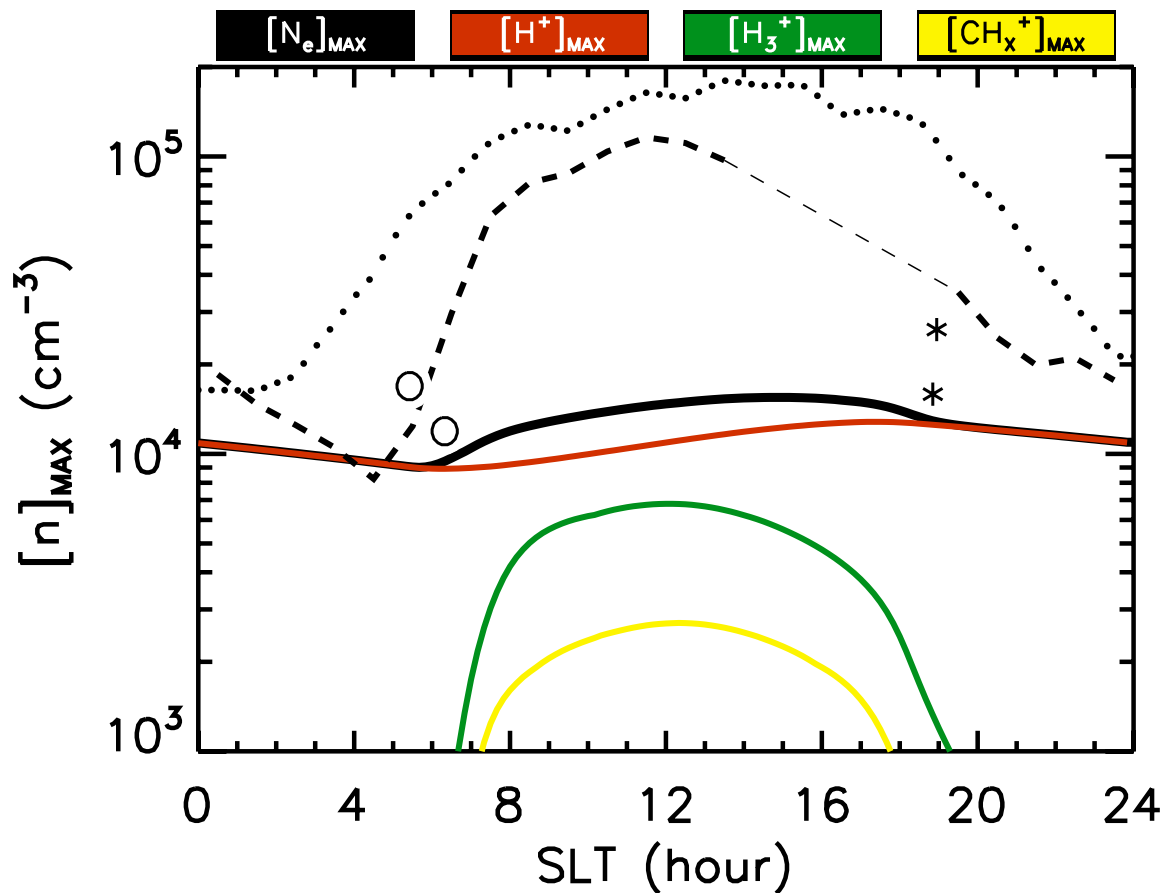
278

## 279 **4. Results: Modeled Diurnal Variations of Electron Density**

### 280 *4.1. Nominal Predictions and Expected Trends*

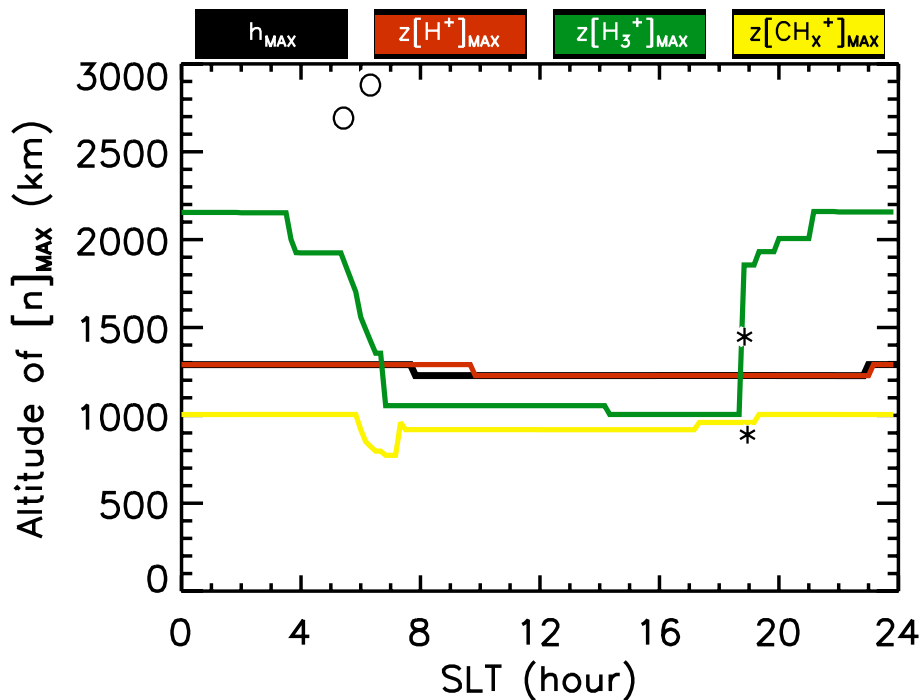
281 Figure 3 presents the nominal model result, based on previous comparisons with  
282 radio occultation observations, for the same conditions described in Figure 4 of Moore et  
283 al. (2010):  $0.125 k_I^*$  and  $\Phi_{eq}$  of  $5 \times 10^6 \text{ cm}^{-2} \text{ s}^{-1}$ . Note that this is actually identical to the  
284  $0.25 k_I^*$  quoted by Moore et al. (2010), as they describe the reduction to the  $k_I$  reaction  
285 rate (by a factor of two) separately from the modification to the population of  
286 vibrationally excited  $\text{H}_2$ , whereas here we incorporate it directly into Eq. (1). Peak  
287 electron density is shown versus solar local time along with the peak densities of the  
288 major ion species. The four radio occultations nearest in latitude to  $35^\circ \text{ S}$  are also shown,  
289 two at dawn (047x and 051x, open circles) and two at dusk (051n and 054n, asterisks).  
290 Table 1 of Kliore et al. (2009) describes the parameters of these occultations in full.  
291 Modeled  $N_{MAX}$  values are within a factor of two of those from radio occultations. A  
292 better model-data agreement could be found for these 4 observations; however, the model  
293 parameters responsible for Figure 3 are based on a comparison with all 31 Cassini radio  
294 occultation profiles (Moore et al., 2010). Finally, two diurnal profiles of  $N_{MAX}$  derived  
295 from Cassini SEDs are also shown in Figure 3: they represent Figure 9 (dotted curve) and  
296 Figure 11 (dashed curve) of Fischer et al. (2011a), respectively. The dotted curve  
297 represents the Cassini  $N_{MAX}$  value when all 231 SED episodes are averaged together,  
298 whereas the dashed curve limits the determination of  $N_{MAX}$  to only SEDs observed when

306 Cassini was within 14  $R_S$  of Saturn. Fischer et al. (2011a) found a slight dependence of  
 307 the cutoff frequency on spacecraft distance (see their Figure 3), and those profiles with  
 308 Cassini nearest to Saturn can be considered as more accurate as the SED intensities are  
 309 higher. The near-distance profiles (i.e. their Figure 11) exhibit a clear minimum in the  
 310 early morning, just before sunrise. Afternoon local times suffer from a lack of data,  
 311 however, and a straight line has been assumed for the  $N_{MAX}$  profile between the 13.5 SLT  
 312 and 19.5 SLT intervals (represented in Figure 3 by a thin dashed line).  
 313  
 314  
 315



306  
 307 **Figure 3.** Nominal STIM results for 35° S latitude, with a solar flux and declination representative of  
 308 Cassini era averages, using  $0.125 k_1^*$  and  $\Phi_0 = 5 \times 10^6 \text{ cm}^{-2} \text{ s}^{-1}$ . Diurnal variation of peak electron density  
 309 ( $N_{MAX}$ ) is given by the black solid curve; red, green and yellow curves represent the peak densities of the  
 310  $H^+$ ,  $H_3^+$  and  $CH_x^+$  ( $= CH_3^+ + CH_4^+ + CH_5^+$ ) ion species, respectively. Also shown are the peak electron  
 311 densities from the four Cassini radio occultation observations nearest to 35° S latitude (047x, 051x, 051n,  
 312 and 054n; Kliore et al., 2009), with open circles for dawn and asterisks for dusk. Finally, the diurnal  
 313 variation of  $N_{MAX}$  derived from Cassini SEDs is also plotted here as dotted and dashed curves (Figure 9 and  
 314 Figure 11, respectively; Fischer et al., 2011a).  
 315

316 As the peak value of individual ion species does not necessarily occur at the  
 317 altitude of the peak electron density,  $h_{\text{MAX}}$ , Figure 4 shows the variation in the peak  
 318 altitude of each ion species, as well as the diurnal variation of  $h_{\text{MAX}}$ . For these simulation  
 319 conditions,  $\text{H}^+$  is the dominant ion near the electron density peak; this shows up clearly in  
 320 Figure 3, and is the reason the red ( $\text{H}^+$ ) and black ( $e^-$ ) curves track each other so closely  
 321 in Figure 4. Dissociative recombination with electrons is the dominant loss of  $\text{H}_3^+$ .  
 322 Therefore, as  $h_{\text{MAX}}$  remains below 1500 km, the increase in the altitude of the  $\text{H}_3^+$  peak  
 323 during the Saturn night is explained by a relatively larger low altitude loss rate leading to  
 324 a high altitude ion ledge just after sunset. Figure 4 serves as a reminder that while we  
 325 plot peak ion densities in Figures 3 and 5, they are at a range of altitudes that differ from  
 326  $h_{\text{MAX}}$ .



327  
 328 **Figure 4.** Nominal STIM results for  $35^\circ$  S latitude, with a solar flux and declination representative of  
 329 Cassini era averages, using  $0.125 k_1^*$  and  $\Phi_0 = 5 \times 10^6 \text{ cm}^{-2} \text{ s}^{-1}$ . Diurnal variation of the altitude of the peak  
 330 electron density ( $h_{\text{MAX}}$ ) is shown in black; red, green and yellow curves represent the altitudes of the peak  
 331 densities of the  $\text{H}^+$ ,  $\text{H}_3^+$  and  $\text{CH}_x^+$  ( $= \text{CH}_3^+ + \text{CH}_4^+ + \text{CH}_5^+$ ) ion species, respectively. Also shown are the  
 332  $h_{\text{MAX}}$  values from the four Cassini radio occultation observations nearest to  $35^\circ$  S latitude (047x, 051x,  
 333 051n, and 054n; Kliore et al., 2009).

334 4.2. Saturn Ionospheric Photochemistry

335 Photoionization of molecular hydrogen is the dominant source of ion production  
336 in Saturn's mid-latitude ionosphere. Approximately 90% of the primary ions produced  
337 through absorption of photons are  $\text{H}_2^+$ , with the remaining 10% of photo ion production  
338 accounting for  $\text{H}^+$ ,  $\text{He}^+$  and hydrocarbon ions. The relatively fast charge exchange  
339 reaction,  $\text{H}_2^+ + \text{H}_2 \rightarrow \text{H}_3^+ + \text{H}$ , means that, effectively,  $\text{H}_3^+$  is the ion most readily  
340 produced in Saturn's ionosphere. Slower production, but typically also slower loss,  
341 allows  $\text{H}^+$  to build up over the course of a few Saturn days, eventually competing with  
342  $\text{H}_3^+$  for dominance in a steady state diurnal solution. The mix of long-lived atomic and  
343 short-lived molecular ions drives the diurnal variation in electron density. As shown by  
344 Moore et al. (2004), the  $\text{H}^+/\text{H}_3^+$  ratio is proportional to electron density in photochemical  
345 equilibrium, which they also demonstrate to hold up to  $\sim 2300$  km in Saturn's mid-latitude  
346 ionosphere. Therefore, for conditions dominated by  $\text{H}^+$ , previous ionospheric models all  
347 predicted a minimal diurnal variation in  $N_{\text{MAX}}$ . On the other hand, in an  $\text{H}_3^+$  dominated  
348 ionosphere, the relatively low photoionization rate at Saturn (i.e., at  $\sim 10$  AU) led to an  
349  $N_{\text{MAX}}$  smaller than derived from SEDs (e.g., Majeed and McConnell, 1996; Moses and  
350 Bass, 2000; Moore et al., 2004).

351 In order to illustrate the difficulty presented in reproducing the SED-derived  
352 diurnal trend in  $N_{\text{MAX}}$ , we consider the following basic calculations. First, the peak  
353 photoionization rate at Saturn during solar maximum conditions for overhead  
354 illumination (i.e., at the sub-solar point) is  $\sim 10 \text{ cm}^{-3} \text{ s}^{-1}$  (Moore et al., 2004). If we take  
355 this maximum production rate to be fixed, and we assume that there are no ion losses  
356 whatsoever, then it would still take 2.5 hours (5.6 Saturn hours) to go from an electron



357 density of  $10^4 \text{ cm}^{-3}$  to  $10^5 \text{ cm}^{-3}$ . Therefore, for Saturn photochemistry to be able to  
358 explain the SED observations, there needs to be a much larger production rate than what  
359 is currently estimated. If we instead start with an electron density of  $10^5 \text{ cm}^{-3}$ , and  
360 require it to decay to  $10^4 \text{ cm}^{-3}$  in  $\sim 6$  Saturn hours (e.g., Figure 9 of Fischer et al., 2011a),  
361 then a different problem presents itself. At 300 K, the approximate temperature near the  
362 ionization peak (e.g., Nagy et al., 2009), the  $\text{H}_3^+$  dissociative recombination rate is on the  
363 order of  $10^7 \text{ cm}^3 \text{ s}^{-1}$ , which means that the decay from  $10^5 \text{ cm}^{-3}$  to  $10^4 \text{ cm}^{-3}$  would take  
364 only  $\sim 30$  Saturn minutes, while the full 6 Saturn hours would find an ionosphere of  $10^3$   
365  $\text{cm}^{-3}$ , too low based on Cassini SED observations. In summary, the largest estimated ion  
366 production rate is clearly not large enough to match the dawn-to-noon increase in  $N_{\text{MAX}}$   
367 derived from SEDs, while a slower ion loss rate is required to match the dusk-to-  
368 midnight decay. Certainly,  $\text{H}^+$  would be expected to have a much slower decay than  $\text{H}_3^+$ ;  
369 however its production rate is roughly a factor of 10 smaller than that of  $\text{H}_3^+$ , which  
370 would further exacerbate the dawn-to-noon discrepancy.

371

#### 372 4.3. Best Match to SED-derived Diurnal Variation of $N_{\text{MAX}}$

373 Figure 3 represents a nearly minimal loss simulation. In other words, the two loss  
374 processes that are not well constrained –charge exchange of  $\text{H}^+$  with  $\text{H}_2\text{O}$  and  $\text{H}_2(v \geq 4)$  –  
375 are already at extremely low values. Even so, the modeled  $N_{\text{MAX}}$  values are significantly  
376 lower than those derived from Cassini era SED observations. Simulations using an  
377 increased solar flux will naturally lead to larger  $N_{\text{MAX}}$  values, though still not as large as  
378 those derived from SEDs (about a factor of two difference in  $N_{\text{MAX}}$  is expected between  
379 solar minimum and solar maximum conditions; Moore et al., 2004). More importantly,

380 those larger fluxes are not justified here, as the measurements were made during a  
 381 prolonged solar minimum period for which the average F10.7 was ~80 (as measured at  
 382 Earth). As argued in Section 4.2, the diurnal variation of  $N_{MAX}$  derived from SEDs  
 383 requires both extremely large production rates and loss rates within one Saturn day.  
 384 Therefore, in the following we show the result of allowing for a wide range of production  
 385 and loss rates (ranging from likely to unrealistic) in order to attempt and answer the  
 386 question: What does it take to reproduce the SED observations?

387 Table 1 summarizes the parameter space explored by the 405 individual 1D model  
 388 simulations that were performed in order to find the combination best able to match the  
 389 SED results. The absolute range of each parameter in Table 1 is described by the  
 390 minimum and maximum values, while the number of different values explored for those  
 391 parameters is given below. Note that the step sizes are variable, with a higher  
 392 concentration of simulations exploring parameters near those that come closest to the  
 393 SED-derived diurnal variation of  $N_{MAX}$ . This results in fewer total model runs than might  
 394 be expected from the number of values evaluated for each parameter.

395 **Table 1.** Range of Simulation Parameters

	$k_1$ * factor <sup>1</sup>	$\Phi_{eq}$ (cm <sup>-2</sup> s <sup>-1</sup> ) <sup>2</sup>	P <sup>3</sup>
<b>Minimum</b>	1	1x10 <sup>6</sup>	1
<b>Maximum</b>	30	4x10 <sup>12</sup>	225
<b>N steps</b>	10	21	13

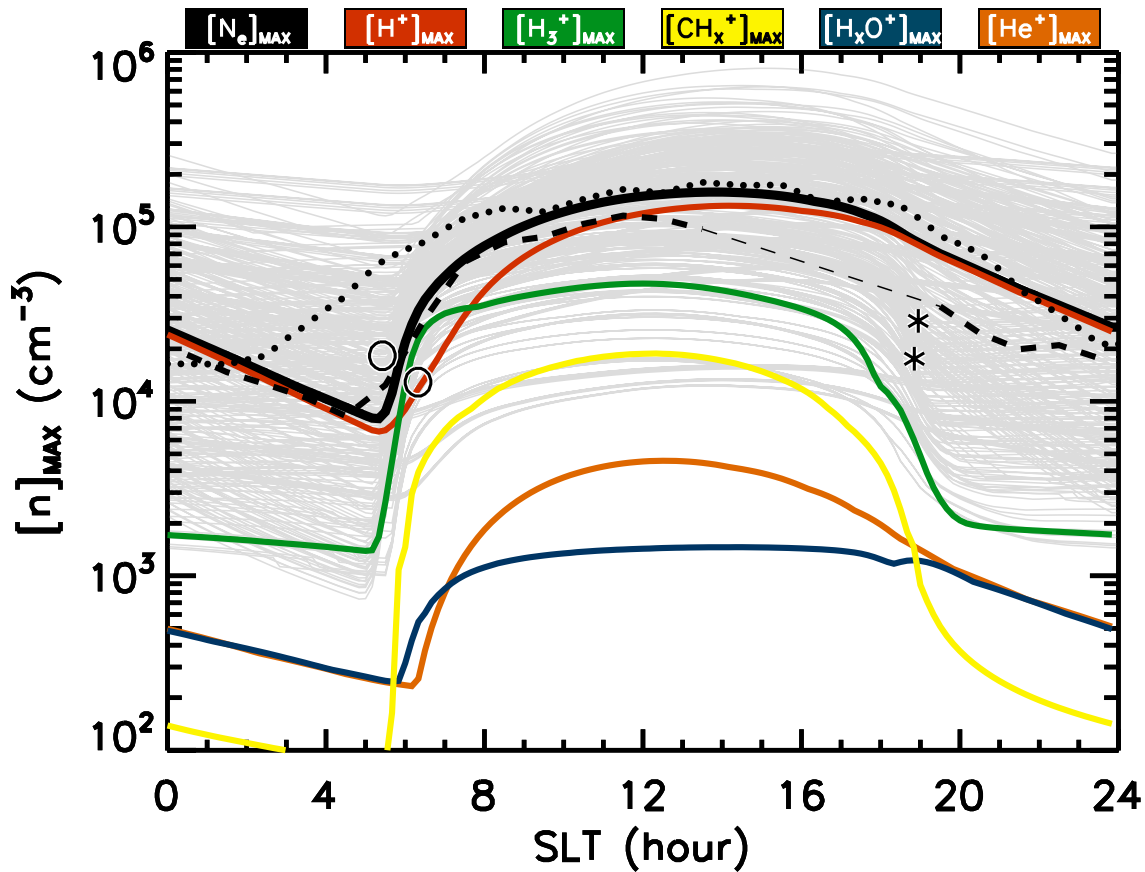
396 <sup>1</sup> See Eq. (1).

397 <sup>2</sup> The water influx at Saturn's equator; as discussed in 3.1, the influx at 35° S latitude is ~0.22% of  $\Phi_{eq}$ .

398 <sup>3</sup> An assumed increase to the ion production rates calculated in the model.

399 Figure 5 shows the model simulation that was best able to reproduce the diurnal  
 400 variation of  $N_{MAX}$ , as derived from Cassini SEDs. Though it is a non-unique solution, it  
 401 is illustrative of the changes in Saturn photochemistry that would be required in order to  
 402 match the observations. The ion production rate – originally due to photoionization and

403 secondary production – has been increased by a factor of 60. In order to balance this  
 404 unphysical production rate, loss rates have also increased significantly: the simulation  
 405 uses  $20 k_I^*$  and  $\Phi_{\text{eq}} = 2.7 \times 10^9 \text{ cm}^{-2} \text{ sec}^{-1}$  (i.e., the water influx at  $35^\circ \text{ S}$  is  $6 \times 10^6 \text{ cm}^{-2}$   
 406  $\text{sec}^{-1}$ ). Without an increase in the nominal ion production rates, it would not be possible  
 407 to go from  $10^4 \text{ e}^- \text{ cm}^{-3}$  at sunrise to  $\sim 10^5 \text{ e}^- \text{ cm}^{-3}$  at noon – a short  $\sim 6$  Saturn hours, or  $\sim 2.6$   
 408 hr. On the other hand, without an increase in the ion loss rates to balance the enhanced  
 409 production rates, Saturn’s ionosphere would have effectively zero diurnal variation.



410  
 411 **Figure 5.** Model simulation (solid lines) that comes closest to reproducing the diurnal variation of  $N_{\text{MAX}}$   
 412 derived from Cassini SEDs (dotted line, Fig. 9 of Fischer et al., 2011a; dashed line, Fig. 11 of Fischer et al.,  
 413 2011a). Calculations are for  $35^\circ \text{ S}$  latitude, with a solar flux and declination representative of Cassini era  
 414 averages. Both the production and loss rates have been significantly enhanced:  $P = 60 P_o$ ,  $20 k_I^*$  and  $\Phi_{\text{eq}} =$   
 415  $2.7 \times 10^9 \text{ cm}^{-2} \text{ s}^{-1}$ . Diurnal variation of the peak electron density ( $N_{\text{MAX}}$ ) is shown in black; red, green,  
 416 yellow, blue, and orange curves represent the peak densities of the  $\text{H}^+$ ,  $\text{H}_3^+$ ,  $\text{CH}_x^+$  ( $= \text{CH}_3^+ + \text{CH}_4^+ + \text{CH}_5^+$ ),  
 417  $\text{H}_x\text{O}^+$  ( $= \text{H}_2\text{O}^+ + \text{H}_3\text{O}^+$ ), and  $\text{He}^+$  ion species, respectively. Gray curves represent the diurnal variation of  
 418  $N_{\text{MAX}}$  from each of the 405 model simulations. Also shown are the  $N_{\text{MAX}}$  values from the four Cassini  
 419 radio occultation observations nearest to  $35^\circ \text{ S}$  latitude (Kliore et al., 2009).  
 420

## 421 **5. Discussion: Other Explanations of the SED-inferred Diurnal Variation of $N_{MAX}$**

422         The comparisons performed above rely on a number of implicit assumptions, such  
423 as: (1) the  $N_{MAX}$  value derived from SEDs is representative of the “main” ionospheric  
424 peak at Saturn, and (2) the low frequency cutoff observed in SEDs occurs in the portion  
425 of the ionosphere directly between the convective storm system and the Cassini  
426 spacecraft. As it is clear now that the diurnal variation of  $N_{MAX}$  derived from Cassini  
427 SED observations can only be reproduced chemically using non-physical ion productions  
428 and losses, it is worthwhile to examine those assumptions more closely.

429

### 430 *5.1. Low-altitude Plasma Layers*

431         The assumption that the  $N_{MAX}$  value derived from SEDs is representative of the  
432 “main” ionospheric peak is particularly important, as the degree of variability seen in the  
433 radio occultations of Saturn’s ionosphere is so large that it is difficult to even define a  
434 “main” ionospheric peak, except on average (Nagy et al., 2006; Kliore et al., 2009).  
435 Moreover, just as at Jupiter (e.g., Yelle and Miller, 2004), a majority of radio occultations  
436 of Saturn’s ionosphere reveal many sharp layers of electron density, especially in the  
437 lower ionosphere, and it is quite common for the peak electron density to be within one  
438 of these layers. A radio wave traversing Saturn’s ionosphere is only sensitive to the  
439 maximum plasma density, not the location of that density, so it is certainly possible that  
440 SEDs are sampling low-altitude sharp ionospheric layers, at least some of the time.

441         Though the origin and evolution of Saturn’s sharp ionospheric layers remain  
442 largely unstudied, a number of possible explanations have been proposed. For example,  
443 Moses and Bass (2000) are able to reproduce the Voyager 2 layers near 1000 km by

444 introducing a shear of  $-2 \text{ cm s}^{-1} \text{ km}^{-1}$  in the vertical plasma drift to act on magnesium  
445 (from dust grains) being deposited in the 790-1290 km region. Such shear could be the  
446 result of ion transport driven by a vertically varying neutral horizontal wind, such as  
447 would result from atmospheric gravity waves. Matcheva et al. (2001) demonstrated that  
448 gravity waves were capable of creating sharp peaks of electron density similar to those  
449 observed by Galileo at Jupiter, and Barrow and Matcheva (2011) greatly expanded this  
450 result, though no similar study has yet been published at Saturn. Finally, plasma  
451 instabilities may also play a role in forming ionospheric layers, though initial estimates of  
452 Rayleigh-Taylor growth periods are  $\sim 4$  hours, comparable to the entire night, meaning  
453 they would not be expected to drive large-scale ionospheric structures at Saturn  
454 (Mendillo et al., 2008).

455         Regardless of their origin, there are a number of conditions that must be met for  
456 these low-altitude layers to be able to explain the  $N_{\text{MAX}}$  values derived from SEDs. First,  
457 either their densities must vary significantly with local time or they must be present only  
458 during the Saturn day. This latter condition represents the possibility that SEDs are  
459 sampling unusually large electron densities from sharp ionospheric layers during the day  
460 and sampling Saturn's "main" ionosphere at night. Second, their densities must correlate  
461 with solar flux, as both the SED-derived diurnal variation and peak  $N_{\text{MAX}}$  value were  
462 shown to correlate with solar EUV flux by Fischer et al. (2011a). Third, they must be  
463 able to be generated at a wide range of latitudes, as sharp low-altitude layers are present  
464 in Cassini radio occultations spanning  $-74.1^\circ$  to  $75.4^\circ$  latitude (Kliore et al, 2009).  
465 Finally, they must be generated on either a constant or a diurnal basis, as all SED storm

466 periods find daytime peak electron densities in excess of  $10^5 \text{ cm}^{-3}$  (Kaiser et al., 1984;  
467 Zarka, 1985, Fischer et al., 2011a).

468

## 469 *5.2. Ring Shadowing*

470 Burns et al. (1983) first posited that the shadows cast by Saturn's rings on its  
471 atmosphere may reduce the local insolation, leading to depleted electron densities, and  
472 thereby providing a possible explanation of the extremely low frequency cutoffs observed  
473 by Voyager. This effect was later studied in more detail, using STIM to calculate the  
474 shadowing effects for both the Voyager and the Cassini eras (Mendillo et al., 2005). The  
475 ring shadowing "solution" to the SED observations essentially relied on the assumption  
476 that SEDs could originate from a range of positions on the planet, and then be ducted  
477 throughout the ionosphere before reaching the detecting spacecraft. Low frequency  
478 cutoffs represented radio waves escaping through ionospheric "holes" caused by ring  
479 shadowing, while high frequency cutoffs represented occasions where the observed radio  
480 waves did not make it to any holes before transiting Saturn's ionosphere.

481 With the Cassini era, however, the situation changed significantly. First, Cassini  
482 was able to identify the location of the SED storms (Dyudina et al., 2007, 2010). This  
483 meant that it was possible to disentangle the path of propagation of the SEDs to some  
484 degree of accuracy. For example, when Cassini was directly above a storm there would  
485 be no ambiguity regarding the portion of Saturn's ionosphere sampled by the SEDs  
486 detected. Second, peak electron densities derived from Cassini low frequency cutoffs  
487 were nearly always above  $10^4 \text{ cm}^{-3}$ , and never as low as  $10^3 \text{ cm}^{-3}$  (Fischer et al., 2011a).  
488 Fischer et al. note that Saturn kilometric radiation (SKR) usually dominates the 300-600

489 kHz frequency band, possibly contaminating the detection of the  $10^3 \text{ cm}^{-3}$  low frequency  
490 cutoffs there. Regardless, the fact that Cassini has not detected such low nighttime  
491 electron densities negates the need for any ring shadowing effects to explain them. It also  
492 implies that either ring shadowing cannot reduce Cassini era electron densities to  $10^3$   
493  $\text{cm}^{-3}$ , contrary to earlier predictions (e.g., Mendillo et al., 2005), or that SEDs are not able  
494 to travel such far distances before escaping through Saturn's ionosphere. Finally, it  
495 should be noted that the Cassini era SED storms ( $35^\circ \text{ S}$  prior to equinox in August 2009,  
496  $35^\circ \text{ N}$  thereafter) have always been located in the opposite hemisphere from the ring  
497 shadowing. There was one exception – an SED storm in the first half of 2010 at  $35^\circ \text{ S}$  –  
498 but it was also located far away from the ring shadow with derived  $N_{\text{MAX}}$  values in  
499 agreement with earlier Cassini storms.

500 In summary, while shadows cast by Saturn's rings could have affected the  
501 ionospheric densities sampled by the equatorial storm of Voyager era SEDs, it seems  
502 unlikely that ring shadowing has played any role for Cassini era SED observations.  
503 Therefore, any explanation of the SED-derived  $N_{\text{MAX}}$  values should be applicable  
504 whether or not ring shadowing effects are present.

505

### 506 *5.3. Plasma Dynamics*

507 Dynamical processes may also impact the electron densities sampled by SEDs,  
508 however the location of the associated storms limits these possibilities significantly. For  
509 instance, the majority of the Cassini era SEDs originate from  $35^\circ \text{ S}$  latitude, which is  
510 magnetically connected to Saturn's C ring at about  $1.44 R_S$ , so it is tempting to imagine a  
511 plasma interchange process occurring between Saturn's ionosphere and ring plane (e.g.,

512 Connerney, 1986). A completely different process would still be required to explain  
513 Voyager era SEDs, however, as they most likely originated from an equatorial storm  
514 system with no magnetic connection to Saturn’s rings. If a dynamical plasma process is  
515 invoked to reproduce diurnal variations of  $N_{MAX}$  from SEDs, it must work equally well at  
516 both mid- and low-latitudes, for both solar minimum and solar maximum flux conditions,  
517 and for conditions with and without ring shadowing.

518

## 519 **6. Summary**

520 We have presented the most comprehensive modeling study to date (405  
521 simulation runs) of the diurnal variation of  $N_{MAX}$  derived from Cassini era SEDs. The  
522 main conclusions are summarized as follows:

523 (1) No combination of Saturn photochemistry can explain the SED  
524 observations when parameters are limited to their observed constraints.

525 (2) Only by introducing artificially large production and loss processes can a  
526 model of Saturn’s photochemical peak reproduce SED observations.

527 (3) SEDs may instead be sampling the highly variable, sharp plasma layers  
528 frequently observed in Saturn’s lower ionosphere, provided those layers  
529 fulfill certain observational constraints.

530 (4) Ring shadowing, first introduced to help explain extremely low  $N_{MAX}$   
531 values from Voyager SEDs, is unlikely to play a role in the Cassini era.

532 Taken together, the first two conclusions are a strong indication that SEDs may  
533 not be sampling Saturn’s “main” ionosphere. It is unlikely that calculated  
534 photoionization rates are off by the factor of 60 used in Figure 5, as they are based on  
535 solar fluxes that have been demonstrated to work well at Earth, and models are able to



536 reproduce the electron densities from radio occultations of Saturn's atmosphere with  
537 much greater accuracy. Similarly, though  $\text{H}_2^*$  and  $\text{H}_2\text{O}$  densities are not completely  
538 constrained at Saturn, the extreme values used in generating Figure 5 are significantly  
539 larger than any previous estimates or observations.

540         The frequency with which low altitude electron density layers are observed in  
541 radio occultations of Saturn (and Jupiter), and the fact that they often represent  $N_{\text{MAX}}$ ,  
542 lends additional credibility to the possibility that SEDs are sampling these highly variable  
543 layers. For such an explanation of the diurnal variation of  $N_{\text{MAX}}$  derived from SEDs to  
544 hold weight, however, it must be demonstrated that they do not violate any of the current  
545 observational constraints. For example, atmospheric gravity waves may indeed be acting  
546 to create such ionospheric structures, as at Jupiter (Barrow and Matcheva, 2011), but: (a)  
547 Are they present at all times during the day and depleted at night? (b) Do their peak  
548 densities correlate with solar EUV flux? (c) Are they present at a wide range of latitudes  
549 and are they present on a near constant basis? Moreover, if gravity waves are responsible  
550 for Saturn's sharp low-altitude layers of electron density: do the wave amplitudes and  
551 periods required to generate  $N_{\text{MAX}}$  values that correspond to those derived from SEDs  
552 violate any other observational constraints? In short, while it is tempting to use these  
553 plasma layers as an explanation of the SED observations, it is yet far from clear that they  
554 can do so adequately.

555

556 *Acknowledgements.*

557 We are grateful to the TIMED/SEE PI Tom Woods, and his team for providing us with  
558 the solar flux data set and associated routines for extrapolation to planets. We

559 acknowledge the contribution of the International Space Sciences Institute (ISSI) in Bern,  
560 Switzerland, for hosting and funding the ISSI International Team on Saturn Aeronomy  
561 (166) and the constructive discussions by colleagues attending the meetings. Funding for  
562 this work at Boston University comes from the NASA CDAP Program. G.F. was  
563 supported by a grant (project P21295-N16) from the Austrian Science Fund (FWF) and  
564 by a short-term research scholarship at the University of Iowa funded by NASA through  
565 contract 1356500 from the Jet Propulsion Laboratory. Partial support for M.G. and  
566 I.M.W. comes from the Science and Technology Facilities Council (STFC) rolling grant  
567 to Imperial College London.

568

## 569 **References**

- 570 Atreya, S.K., Waite, J.H., Donahue, T.M., Nagy, A.F., and McConnell, J.C., 1984. Theory, measurements  
571 and models of the upper atmosphere and ionosphere of Saturn. In: Gehrels, E. (Ed.), Saturn, Univ. of  
572 Ariz. Press, Tucson, 239-277.
- 573 Barrow, D. and Matcheva, K.I., 2011. Impact of atmospheric gravity waves on the jovian ionosphere.  
574 Icarus 211, 609-622.
- 575 Burns, J.A., Showalter, M.R., Cuzzi, J.N., and Durisen, R.H., 1983. Saturn's electrostatic discharges -  
576 Could lightning be the cause? Icarus 54, 280-295.
- 577 Connerney, J.E.P. and Waite, J.H., 1984. New model of Saturn's ionosphere with an influx of water from  
578 the rings. Nature 312, 136-138.
- 579 Connerney, J.E.P., 1986. Magnetic connection for Saturn's rings and atmosphere. Geophysical Research  
580 Letters 13, 773-776.
- 581 Davis, L., Jr. and Smith, E.J., 1990. A model of Saturn's magnetic field based on all available data.  
582 Journal of Geophysical Research 95, 15257-15261.
- 583 Dyudina, U.A., and 6 colleagues, 2010. Detection of visible lightning on Saturn. Geophysical Research  
584 Letters 37, L09205, doi:10.1029/2010GL043188.
- 585 Dyudina, U.A., and 9 colleagues, 2007. Lightning storms on Saturn observed by Cassini ISS and RPWS  
586 during 2004-2006. Icarus 190, 545-555.
- 587 Evans, D.R., Romig, J.H., Hord, C.W., Simmons, K.E., Warwick, J.W., and Lane, A.L., 1982. The source  
588 of Saturn electrostatic discharges. Nature 299, 236-237.
- 589 Evans, D.R., Warwick, J.W., Pearce, J.B., Carr, T.D., and Schauble, J.J., 1981. Impulsive radio discharges  
590 near Saturn. Nature 292, 716-718.
- 591 Fischer, G., and 10 colleagues, 2006. Saturn lightning recorded by Cassini/RPWS in 2004. Icarus 183,  
592 135-152.
- 593 Fischer, G., and 7 colleagues, 2007. Analysis of a giant lightning storm on Saturn. Icarus 190, 528-544.
- 594 Fischer, G., and 7 colleagues, 2008. Atmospheric Electricity at Saturn. Space Science Reviews 137, 271-  
595 285.
- 596 Fischer, G., Gurnett, D.A., Zarka, P., Moore, L., and Dyudina, U.A., 2011a. Peak electron densities in  
597 Saturn's ionosphere derived from the low-frequency cutoff of Saturn lightning. Journal of  
598 Geophysical Research (Space Physics) 116, A04315, doi:10.1029/2010JA016187.

599 Fischer, G., and 10 colleagues, 2011b. A giant thunderstorm on Saturn. *Nature* 475, 75-77.

600 Galand, M., Moore, L., Charnay, B., Müller-Wodarg, I., and Mendillo, M., 2009. Solar primary and  
601 secondary ionization at Saturn. *Journal of Geophysical Research (Space Physics)* 114, A06313,  
602 doi:10.1029/2008JA013981.

603 Galand, M., Moore, L., Müller-Wodarg, I., Mendillo, M., and Miller, S., 2011. Response of Saturn's  
604 auroral ionosphere to electron precipitation: Electron density, electron temperature, and electrical  
605 conductivity. *Journal of Geophysical Research (Space Physics)* 116, A09306,  
606 doi:10.1029/2010JA016412.

607 Huestis, D.L., 2008. Hydrogen collisions in planetary atmospheres, ionospheres, and magnetospheres.  
608 *Planetary and Space Science* 56, 1733-1743.

609 Kaiser, M.L., Connerney, J.E.P., and Desch, M.D., 1983. Atmospheric storm explanation of saturnian  
610 electrostatic discharges. *Nature* 303, 50-53.

611 Kaiser, M.L., Desch, M.D., and Connerney, J.E.P., 1984. Saturn's Ionosphere: Inferred electron densities.  
612 *Journal of Geophysical Research*, 89, A4, 2371-2376.

613 Kliore, A.J., and 6 colleagues, 1980. Structure of the Ionosphere and Atmosphere of Saturn From Pioneer  
614 11 Saturn Radio Occultation, *Journal of Geophysical Research*, 85, A11, 5857-5870.

615 Kliore, A.J., and 6 colleagues, 2009. Midlatitude and high-latitude electron density profiles in the  
616 ionosphere of Saturn obtained by Cassini radio occultation observations. *Journal of Geophysical  
617 Research (Space Physics)* 114, A04315, doi:10.1029/2008JA013900.

618 Lindal, G.F., D.N. Sweetnam, and V.R. Eshleman, 1985. The Atmosphere of Saturn: An Analysis of the  
619 Voyager Radio Occultation Measurements. *Astronomical Journal* 90, 1136-1146.

620 Majeed, T. and McConnell, J.C., 1996. Voyager electron density measurements on Saturn: Analysis with a  
621 time dependent ionospheric model. *Journal of Geophysical Research* 101, 7589-7598.

622 Matcheva, K.I., Strobel, D.F., and Flasar, F.M., 2001. Interaction of Gravity Waves with Ionospheric  
623 Plasma: Implications for Jupiter's Ionosphere. *Icarus* 152, 347-365.

624 McElroy, M.B., 1973. The Ionospheres of the Major Planets. *Space Science Reviews* 14, 460-473.

625 Melin, H., Miller, S., Stallard, T., Trafton, L.M., and Geballe, T.R., 2007. Variability in the H<sub>3</sub><sup>+</sup> emission  
626 of Saturn: Consequences for ionisation rates and temperature. *Icarus* 186, 234-241.

627 Mendillo, M., Moore, L., Clarke, J., Müller-Wodarg, I., Kurth, W.S., and Kaiser, M.L., 2005. Effects of  
628 ring shadowing on the detection of electrostatic discharges at Saturn. *Geophysical Research Letters*  
629 32, L05107, doi:10.1029/2004GL021934.

630 Mendillo, M., and 9 colleagues, 2008. Can Equatorial Spread-F (ESF) Occur on Other Planets? ISEA 2008  
631 Abstracts S6-P2-31.

632 Moore, L.E., Mendillo, M., Müller-Wodarg, I.C.F., and Murr, D.L., 2004. Modeling of global variations  
633 and ring shadowing in Saturn's ionosphere. *Icarus* 172, 503-520.

634 Moore, L., Nagy, A.F., Kliore, A.J., Müller-Wodarg, I., Richardson, J.D., and Mendillo, M., 2006. Cassini  
635 radio occultations of Saturn's ionosphere: Model comparisons using a constant water flux.  
636 *Geophysical Research Letters* 33, L22202, doi:10.1029/2006GL027375.

637 Moore, L. and Mendillo, M., 2007. Are plasma depletions in Saturn's ionosphere a signature of time-  
638 dependent water input? *Geophysical Research Letters* 34, L12202, doi:10.1029/2007GL029381.

639 Moore, L., Galand, M., Müller-Wodarg, I., Yelle, R., and Mendillo, M., 2008. Plasma temperatures in  
640 Saturn's ionosphere. *Journal of Geophysical Research (Space Physics)* 113, A10306,  
641 doi:10.1029/2008JA013373.

642 Moore, L., Galand, M., Müller-Wodarg, I., and Mendillo, M., 2009. Response of Saturn's ionosphere to  
643 solar radiation: Testing parameterizations for thermal electron heating and secondary ionization  
644 processes. *Planetary and Space Science* 57, 1699-1705.

645 Moore, L., Müller-Wodarg, I., Galand, M., Kliore, A., and Mendillo, M., 2010. Latitudinal variations in  
646 Saturn's ionosphere: Cassini measurements and model comparisons. *Journal of Geophysical  
647 Research (Space Physics)* 115, A11317, doi:10.1029/2010JA015692.

648 Moses, J.I. and Bass, S.F., 2000. The effects of external material on the chemistry and structure of Saturn's  
649 ionosphere. *Journal of Geophysical Research* 105, 7013-7052.

650 Müller-Wodarg, I.C.F., Mendillo, M., Yelle, R.V., and Aylward, A.D., 2006. A global circulation model of  
651 Saturn's thermosphere. *Icarus* 180, 147-160.

652 Müller-Wodarg, I.C.F., L. Moore, M. Galand, and M. Mendillo, Magnetosphere-Atmosphere Coupling at  
653 Saturn: 1. Response of Thermosphere and Ionosphere to Steady State Polar Forcing, *submitted to  
654 Icarus*, 2012.

655 Nagy, A.F., and 11 colleagues, 2006. First results from the ionospheric radio occultations of Saturn by the  
656 Cassini spacecraft. *Journal of Geophysical Research (Space Physics)* 111, A06310,  
657 doi:10.1029/2005JA011519.

658 Nagy, A.F., Kliore, A.J., Mendillo, M., Miller, S., Moore, L., Moses, J.I., Müller-Wodarg, I., and  
659 Shemansky, D., 2009. Upper atmosphere and ionosphere of Saturn, In: Dougherty, M.K., Esposito,  
660 L.W., and Krimigis, S.M. (Eds.), *Saturn From Cassini-Huygens*, Springer, New York, 181-202.

661 Porco, C.C., and 34 colleagues, 2005. Cassini Imaging Science: Initial Results on Saturn's Atmosphere.  
662 *Science* 307, 1243-1247.

663 Russell, C.T. and Dougherty, M.K., 2010. Magnetic Fields of the Outer Planets. *Space Science Reviews*  
664 152, 251-269.

665 Smith, G.R., Shemansky, D.E., Holberg, J.B., Broadfoot, A.L., Sandel, B.R., and McConnell, J.C., 1983.  
666 Saturn's upper atmosphere from the Voyager 2 EUV solar and stellar occultations. *Journal of*  
667 *Geophysical Research* 88, 8667-8678.

668 Spilker, L.J., 2012. Cassini: Science Highlights from the Equinox and Solstice Missions. *Lunar and*  
669 *Planetary Institute Science Conference Abstracts* 43, 1358.

670 Tyler, G.L., and 6 colleagues, 1981. Radio science investigations of the Saturn system with Voyager 1 -  
671 Preliminary results. *Science* 212, 201-206.

672 Warwick, J.W., and 12 colleagues, 1981. Planetary radio astronomy observations from Voyager 1 near  
673 Saturn. *Science* 212, 239-243.

674 Warwick, J.W., and 9 colleagues, 1982. Planetary radio astronomy observations from Voyager 2 near  
675 Saturn. *Science* 215, 582-587.

676 Woods, T., and 9 colleagues, 2000. TIMED Solar EUV experiment. *Physics and Chemistry of the Earth C*  
677 25, 393-396.

678 Woods, T.N., and 8 colleagues, 2005. Solar EUV Experiment (SEE): Mission overview and first results.  
679 *Journal of Geophysical Research (Space Physics)* 110, A01312, doi:10.1029/2004JA010765.

680 Woods, T.N., 2008. Recent advances in observations and modeling of the solar ultraviolet and X-ray  
681 spectral irradiance. *Advances in Space Research* 42, 895-902.

682 Yelle, R.V., and Miller, S., 2004. Jupiter's thermosphere and ionosphere, In: Bagenal, F., Dowling, T.E.,  
683 McKinnon, W.B. (Eds.), *Jupiter: The Planet, Satellites and Magnetosphere*, Cambridge Univ. Press,  
684 New York, 185-218.

685 Zarka, P. and Pedersen, B.M., 1983. Statistical study of Saturn electrostatic discharges. *Journal of*  
686 *Geophysical Research* 88, 9007-9018.

687 Zarka, P., 1985. Directivity of Saturn electrostatic discharges and ionospheric implications. *Icarus* 61,  
688 508-520.

689 Zarka, P., Cecconi, B., Denis, L., Farrell, W.M., Fischer, G., Hospodarsky, G.B., Kaiser, M.L., Kurth,  
690 W.S., 2006. Physical properties and detection of Saturn's radio lightning. In: *Planetary Radio*  
691 *Emissions VI*, edited by Rucker, H.O., Kurth, W.S., Mann, G., Austrian Academy of Sciences Press,  
692 111-122.